Advanced Theory and Simulations

Recommendation System to Predict the d-band Center of Core-Shell bimetallic NanoparticlesCatalysts

--Manuscript Draft--

Manuscript Number:	adts.202401460
Article Type:	Research Article
Corresponding Author:	Abhishek Singh Indian Institute of Science Bangalore, INDIA
Order of Authors (with Contributor Roles):	Sakshi Agarwal, PhD (Conceptualization: Supporting; Data curation: Equal; Validation: Equal; Writing – original draft: Equal; Writing – review & editing: Equal)
	Abhishek Singh (Conceptualization: Lead; Data curation: Equal; Funding acquisition: Lead; Project administration: Lead; Writing – original draft: Equal; Writing – review & editing: Equal)
Keywords:	Nanocatalysts; Machine Learning; DFT calculations; core-shell nanoparticles; d-band centre
Abstract:	Core-shell nanoparticles are an important class of catalytic materials due to synergistic effect of more than one elements. Exploring the electronic properties such as the d-band center (d) and the related catalytic properties of these materials are quite challenging due to resource consuming experiments and computationally expensive modeling of the nanoparticles. We developed a density functional theory (DFT) coupled recommendation system based approach to predict the d of the core-shell nanoparticles. The recommendation system involves completion of a core-shell interaction matrix, where each matrix element represents the d of a unique core-shell pair. Matrix completion by predicting the interaction matrix elements was carried out using neural network. The neural network generated a low dimensional representations for each core and shell metals, which were learned iteratively to predict corresponding d of the pair. The learned representations brilliantly captures the similarities and dissimilarities between metals present in shell or core. The same model has further been employed to predict thed-band width (w), suggesting its transferability. This approach recommends the optimum range of d/ w along with the combination of core-shell metals having most efficient adsorption of species for any reaction.

RESEARCH ARTICLE

Recommendation System to Predict the d-band Center of Core-Shell bimetallic Nanoparticles Catalysts

Sakshi Agarwal[1*] | **Abhishek Singh**[1*]

[1]Materials Research Centre, Bangalore, Karnataka 560012, India

Correspondence
Abhishek Singh, Materials Research Centre, Bangalore, Karnataka 560012, India
Email: abhishek@iisc.ac.in

Funding information
Science and Engineering Research Board (SERB), Department of Science and Technology (DST), Government of India. DST-Nanomission programme of Department of Science and Technology, Government of India

Core-shell nanoparticles are an important class of catalytic materials due to the presence of unsaturated bonds, phase-separated metals, and synergistic effect of more than one elements. Exploring the electronic properties such as the d-band center (ϵ_d) and the related catalytic properties of these materials are quite challenging due to resource consuming experiments and computationally expensive modeling of the nanoparticles. Therefore, we developed a density functional theory (DFT) coupled recommendation system based approach to predict the ϵ_d of the core-shell nanoparticles. Here, the recommendation system involves completion of a core-shell interaction matrix, where each matrix element represents the ϵ_d of a unique core-shell pair. Matrix completion by predicting the interaction matrix elements was carried out using neural network. The neural network generated a low dimensional representations for each core and shell metals, which were learned iteratively to predict corresponding ϵ_d of the pair. The learned representations brilliantly captures the similarities and dissimilarities between metals present in shell or core. A very low train/test RMSE of 0.009/0.009 is obtained with elemental features based model. The same model has further been employed to predict the d-band width (ϵ_w), suggesting its transferability.

This approach recommends the optimum range of ϵ_d / ϵ_w along with the combination of core-shell metals having most efficient adsorption of species for any reaction. The results presented in this study can help experimentally design the core-shell nanoparticles having a desired catalytic activity.

KEYWORDS

Density functional theory, machine learning, recommendation system, d-band center, d-band width

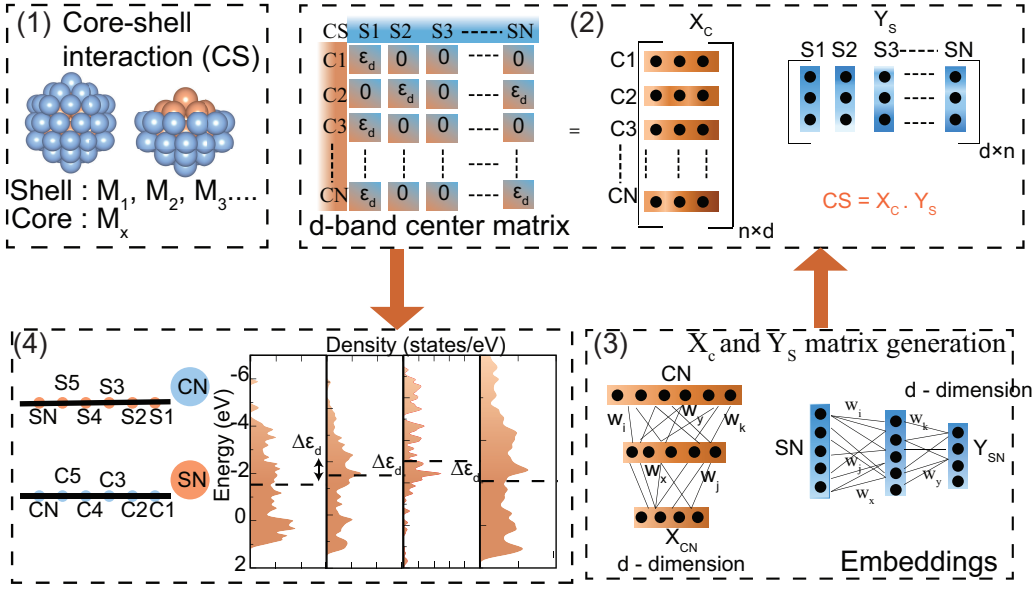

FIGURE 1 The recommendation system workflow (1) showing the core-shell icosahedra structure, (2) the core-shell interaction matrix for all the core-shell element combinations, (3) the d-dimensional embedding matrix for each core and shell generated from a neural network with input and hidden layers, and (4) prediction of the d-band center using the completion of the interaction matrix by the learned embedding

1 | INTRODUCTION

Catalysis plays a vital role in industrialising a reactive process by accelerating the rate of the reaction. Heterogeneous catalysts based on transition metals is an important class of catalysis because of their exceptional activity due to the presence of d−orbitals[1]. Furthermore, with the advent of sophisticated synthesis techniques, the alloyed nanoparticles with precisely defined atomic arrangements, such as single-atom alloys[2, 3], intermetallic structures[4], and core−shell materials emerged as a dominant category of the TM heterogeneous catalysis [5, 6, 7]. Due to versatility

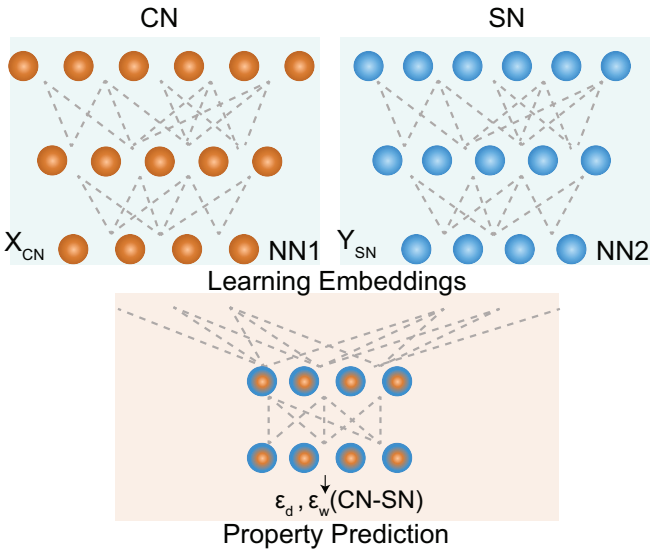

FIGURE 2 The neural network architecture to generate lower dimension embeddings (NN1 and NN2), which acts as an input to second neural network in order to predict ϵ_d and ϵ_w.

of compositions, which in turn tune the catalytic properties, core-shell nanostructures are gaining significant attention. Core-shell nanoparticles offer new properties due to the synergisitc interactions between the core and shell metals[8]. They are commonly synthesized using the seeded mechanism, which can lead to nanoparticles of different sizes and shapes[8, 9]. In addition, based on the presence of one, two, and more elements in the core, the core-shell nanoparticles can be bimetallic, trimetallic and multimetallic, respectively. As a result, a wide variety of catalysts can be developed.

Exploring the catalytic activity of core-shell nanoparticles with numerous possible combinations of core and shell elements via conventional approaches is energy and resource-intensive task. Despite successful demonstrations of core-shell catalysts in electrocatalysis[10, 11, 12, 13], a very few theoretical and experimental studies systematically link the metal distribution to the catalysts performance[14, 15]. On the other hand, computational modeling of the catalytic materials accelerated the search for efficient catalysts due to the existence of Sabatiers principle, scaling laws, and the Bronsted-Evans-Polanyi (BEP) relationship, which directly correlate the intrinsic properties of catalysts and the thermodynamics of the reaction[16, 17]. Therefore, it is quite advantageous to use the characteristics electronic properties of the core-shell catalytic materials to comprehend their effectiveness in catalyzing reactions[18, 19, 20]. The d-band centre (ϵ_d)[20, 21, 22], d-band width (ϵ_w)[23], d-band shape [24], and coordination number[25, 26], are the most frequently utilised properties to characterise the catalytic efficiency. Out of which, ϵ_d is considered as an universal and accurate property of a catalyst for defining the thermodynamics of a reaction[27, 18, 19, 20]. It helps to understand how effectively a catalyst material may bind the adsorbate molecule. It suggests that the closer the ϵ_d to the Fermi-level, the stronger the adsorption[20, 21, 22, 7, 28, 29]. Based on the adsorption of the reaction intermediates effectiveness of a catalyst towards a reaction can be anticipated. Additionally, the width of the d-band, can further reveal details about the complex interactions of the adsorbate molecule with the nanoparticle catalyst. However, calculating these intrinsic properties for each combination of core-shell catalyst and correlating its behavior with the catalyst's efficiency is resource extensive and time consuming. Designing nanoparticle catalysts may benefit

greatly from a novel strategy that combines theoretical models with data-based approach. Recently, machine learning

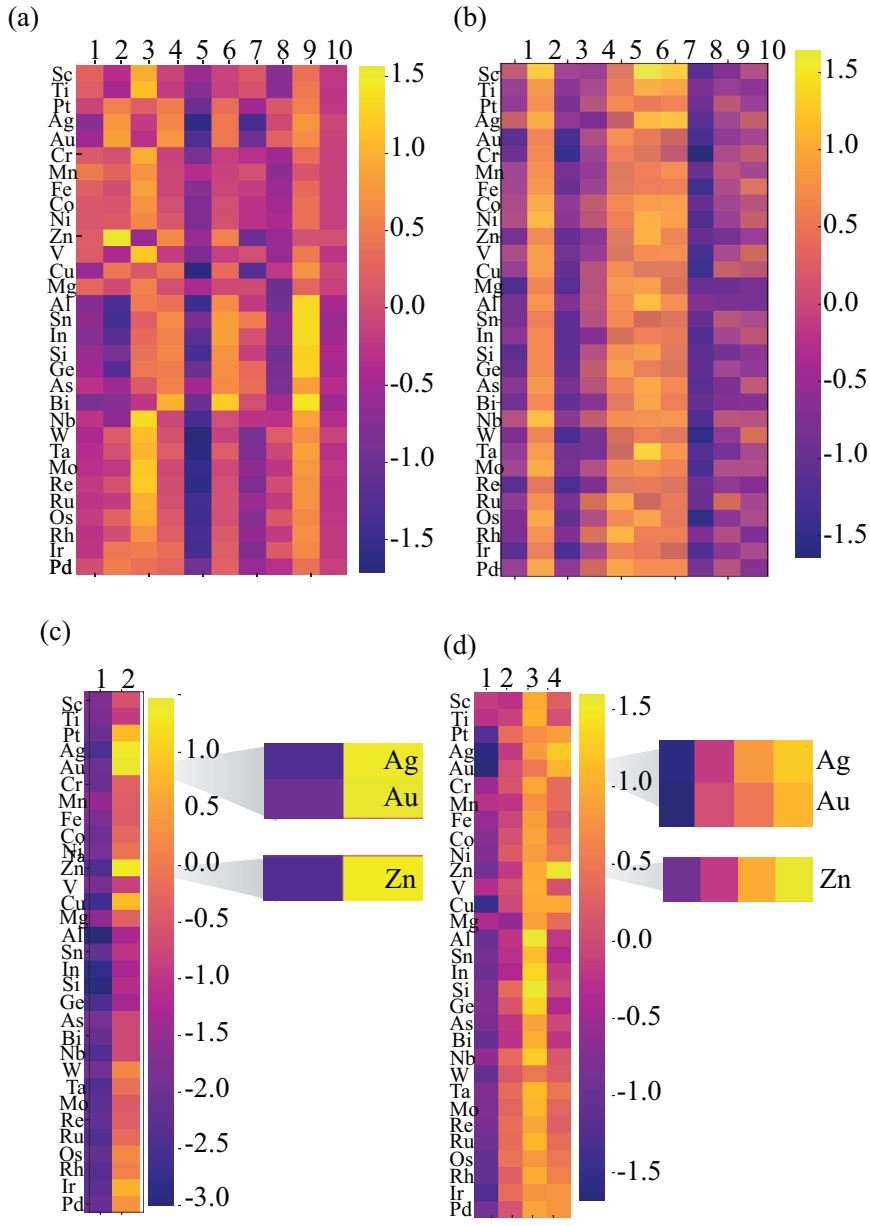

FIGURE 3 The representation heat maps at four different dimensions for each core elements (a) ten-dimensional embedding representations using model 1, (b) ten-dimensional embedding representations using model 2, (c) two-dimensional embeddings, and (d) four-dimensional embeddings.

(ML) based techniques have become a potent tool for materials design and prediction of various complex properties

of materials[30, 31, 32, 33, 34, 35, 36]. A new branch of machine learning based on recommendations is extremely popular in e-commerce and entertainment platforms. This approach has a potential applications for material design due to its ability to predict the pairwise preference of two interdependent species.[37, 38, 39, 40, 41, 42, 43, 44].

Here, we applied this approach to predict the ϵ_d of the interrelated elements in core-shell nanoparticles. Upon calculation of the ϵ_d for few random combinations of core-shell nanoparticles using density functional theory (DFT), the recommendation system is used to predict the ϵ_d for all the combinations of core-shell nanoparticles. It involves formation of an interaction matrix with each matrix element representing ϵ_d of a unique pair. The prediction of the matrix elements requires generation of representations for each core and shell elements, which are learned iteratively using neural network. The learned representation further elucidates the similarities among the various elements when present as core or shell in the nanoparticle. The recommendation system efficiently captures the change in ϵ_d with the change in core or shell elements. To further examine the transferability and performance of the model the ϵ_w of the same dataset was predicted. This ML-based approach provides a simpler and faster way to reliably predict and recomends desired pairwise properties of materials.

2 | METHODOLOGY

DFT calculations: First principle calculations are performed using density functional theory (DFT) as implemented in the Vienna *ab initio* simulation package (VASP) [45]. Electron-ion interactions are described by all electron projector augmented wave (PAW) pseudopotentials [46] and the electronic exchange and correlations were approximated by a Perdew-Burke-Ernzerhof (PBE) generalized gradient approximation (GGA) [47] including spin polarization effects. The periodic images were separated by a 15 Å vacuum along all directions to prevent spurious interactions. For structure optimization, the Brillouin zone was sampled by a Γ point. All structures were fully relaxed using a conjugate gradient scheme until the energies and each component of forces were less than 10^{-6} eV and 0.01 eV Å^{-1}, respectively. The kinetic energy cut off of plane waves is set to 400 eV.

3 | RESULTS AND DISCUSSION

We have selected 55 atoms (13-core, 42-shell) core-shell nanoparticles with icosahedral geometry, which is the most observed structure for TMs. The 42 atom shell encapsulates 13 atoms core, both in icosahedral framework. Core and shell metals are chosen from a broad spectrum of 31 widely used elements in catalysis belonging to the $3d$, $4d$, $5d$ series of transition metals. Additionally, elements such as Mg, Al, Sn, In, Si, Ge, As, and Bi from the $p-$block are also considered in the study to see their effect on the d-band center and d-band width. All the elements considered in this study are shown in Figure S1. Each element can be present in both core and shell. Since, the number of core and shell elements in the nanoparticle is different, each pair of elements will give two different structures. Hence, there is no duplication in the data. A total of ∼1000 nanoparticles are generated. The machine learning model is chosen in such a way that it captures the pairwise preference and the interdependence of core and shell elements. The ϵ_d of shell elements gets altered due to the presence of different core elements. This work aims to predict this change in ϵ_d of shell elements and recommend elements in the core and shell with preferred ϵ_d values. A neural network-based recommendation system is employed for the prediction of this interrelated property of the core and shell elements. The first step of this approach is generating the input data for the recommendation model. Therefore, using DFT, the nanoparticle's geometries were optimized, followed by the calculation of d-band center. However, for core-shell nanoparticles, optimizing the structures and calculating the d-band center is a computationally expensive

process. This problem was effectively addressed through the use of a recommendation system, which was particularly well-suited for low-data environments. The recommendation system leverages patterns and similarities from limited data, allowing it to make accurate predictions and provide reliable insights even when data availability is constrained. Therefore, 20% random structures of the total data were selected. The data generated ensures that the core and shell elements in the study are well-represented, even with this reduced data size. Once the data is generated the next step involves the creation of an interaction matrix for the core and shell elements.

Core-shell interaction matrix (CS) of dimensions n x n is generated, where n represents the total number of elements under study, i.e., 31. Each element of the 31 x 31 interaction matrix represents the ϵ_d of the combination of 31 core and shell elements. For instance, ϵ_{C1S1} represents the ϵ_d of S1 shell element with C1 core element (Figure 1). Initially, the interaction matrix contains the 20% DFT calculated values of ϵ_d, and the remaining matrix elements were considered as zero. Each row and column contains representative d-band center values for each element calculated using DFT. The missing values are to be predicted using the known ones by generating a pseudo-interaction matrix with all the ϵ_d values for each pair. Therefore, the primary objective of the recommendation system is the completion of this interaction matrix (Figure 1) to a pseudo interaction matrix.

The matrix completion based on neural networks is employed to perform the task of predicting the approximated pseudo-interaction matrix. In Matrix completion, the interaction matrix for core and shell elements is represented by two lower-dimensional matrices (X_C and Y_S) as shown in Figure 1. Two different methods are selected to provide the basis for the two lower dimensional matrices. The first method (model 1) involves the elemental features of the elements as the initial input of the X_C and Y_S matrices. The set of elemental representations for the model 1 composed of the (1) atomic number, (2) atomic mass, (3) period, (4) group in the periodic table, (5) first ionization energy, (6) second ionization energy, (7) electron affinity, (8) Pauling electronegativity, (9) Allen electronegativity, (10) van der Waals radius, (11) covalent radius, (12) atomic radius, (13) melting point, (14) boiling point, (15) density, (16) molar volume, (17) heat of fusion, (18) heat of vaporization, (19) thermal conductivity, (20) specific heat, and (21) number of d-electrons. These representations contain the physical properties of elements forming the core and shell. On the other hand, in model 2, the input of the X_C and Y_S matrices are randomly generated vectors. These lower-dimensional matrices generated from both models provide representations for each core and shell element (Figure 1), also known as element embedding. It can be seen from Figure 1 that matrix completion is done in such a way that core element embedding is in the form of a row matrix and a column matrix for shell elements. For model 1, to differentiate between the representation of a element when present in core or shell, a column of zeroes and row of ones are padded in the row and column matrix of core and shell elements, respectively. For instance, in Figure 1, C1 represents the embedding for element 1, and S1 is the embedding of corresponding shell element 1.

To enable machines to acquire knowledge about the core and shell atoms beyond the raw input data statistics, a neural network (NN) is employed to learn and reduce the dimensions of the representations or embeddings for both core (X_C) and corresponding shell elements (X_S). Two separate neural networks are implemented in both models for transforming X_C (NN1) and Y_S (NN2) as shown in Figure 2. Neural networks consists of artificial neurons that are arranged layer by layer, and adjacent layers are fully coupled using a linear transformation. The weights and bias between layers are optimized to minimize the loss function over the training dataset. Each neural networks consists of input, output, and two hidden layers. The hidden layer consists of 10 neurons, where the neurons in intermediate hidden layers are subjected to nonlinearity function rectified gated linear units (ReLU). The root mean-square error (RMSE) of prediction is used as a loss function. In model 1, the concatenation of 21 elemental feature vectors from the i^{th} core element (C_i) or shell element (S_i) serves as the input layer, where i = 1, 2, 3....31. On the other hand, in model 2, a 21-dimensional random vector is created as an input to both the neural network. The input layer for each model is fully connected to two hidden layer equipped with nonlinear activation as shown in Figure 2. To identify the

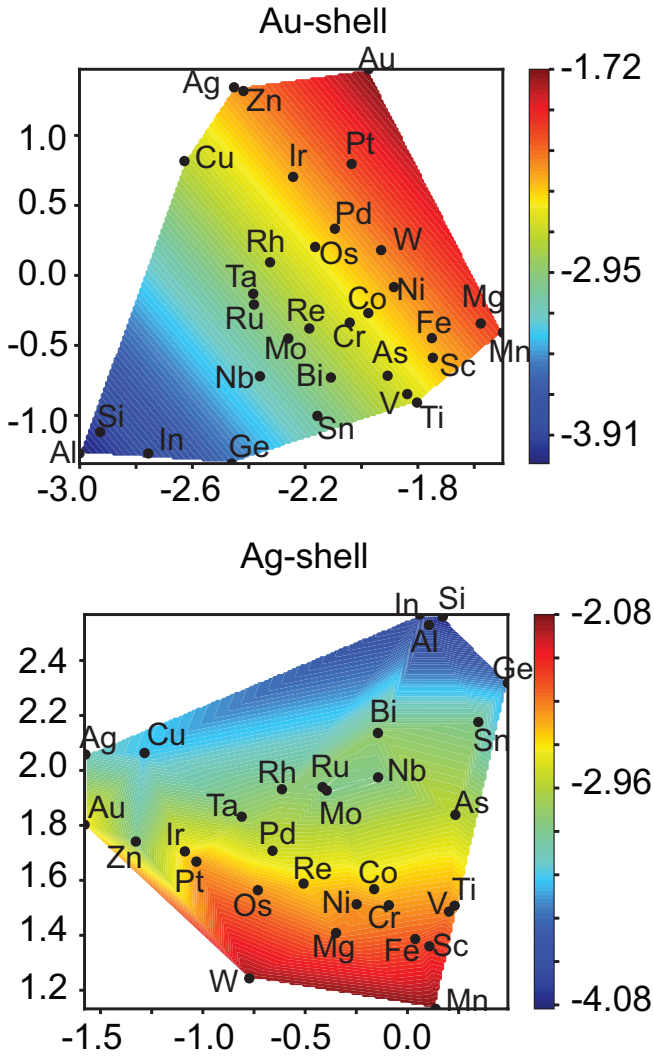

FIGURE 4 Contour plots between the two dimensions for each d-dimensional embeddings with the predicted ϵ_d. The color bar indicate the values of predicted ϵ_d of Au and Ag with change in core-elements.

best-performing network, different amounts of neurons are applied in the hidden layer in front of the single output neuron. The dimensions of the embeddings depends directly on the number of hidden neurons. These embeddings are abstract numerical values that the network uses to capture the features of the elements, and they reflect the relationships or similarities between different elements based on the model's learning process. Since these weights do not correspond to physical quantities, they are dimensionless and do not have units. To understand how well the different dimensional embeddings capture the properties of elements, we examined the learned embeddings of core and shell for the range of dimensions (d). Figure 3(a) illustrates a 10 dimensional embedding generated by model 1, where distinct patterns of different core element vectors in the heatmap are depicted. The heatmaps clearly indicate

similarities and dissimilarities between elements of the same group/period. For instance, it is observed that there exist similarities between the embeddings of p-block elements and metals belonging to the same group of the d-block. Although, the embeddings are not exactly identical, which is due to difference in the physical and chemical properties of elements as we go down the group. As a result, their effect on the ϵ_d of the core-shell pair also differs. Furthermore, it can be seen that the embedding can efficiently capture the uniqueness of zinc from all the elements due to its d^{10} configuration. The embeddings for Pd and Pt are similar to each other but shows distinct difference with embedding of Ni. This is attributed to the fact that the properties of Pd and Pt are similar to each other compared to Ni. The electronic configuration, i.e., the number of d-electrons itself changes as we move from Ni to Pd and Pt. As a result, the ionization energies, electron affinity, and electronegativity are quite dissimilar. However, it is also clear from the Figure 3(b) that the embeddings generated from model 2 are unable to capture these detailed information. For instance, the similarities between the metals of copper family are not captured in the embeddings generated from model 2. Therefore, from Figure 3(a and b), we concluded that model 1 outperforms model 2 in terms of capturing the intrinsic information about the elements. Representation generated using model 1 ought to be parametrically dependent on the kind of elements used for the core or shell, providing insights into the intrinsic nature of elements.

Further, a higher dimensional embedding can increase the model complexity, therefore, for a simpler model, dimensions of embedding are varied from 10 to 2. As shown in Figure 3(c), for d=2, there is a compromise in the enclosed information. The similarity between some metals, such as Ag and Au, are clearly captured by a two-dimensional vector. However, the dissimalrity between Zn and Ag is not adequately depicted. On the other hand, a four dimensional embedding in Figure 3(d) can efficiently find the patterns of similarities and dissimilarities among the representations of the elements. In addition, a reduction in the RMSE value is observed with lower d, suggesting that lower dimensional embedding performs better to fit the data as shown in Figure S1 (a). The high dimensional embedding would be difficult to employ for a smaller dataset as the model tries to overfit. Therefore, above discussion suggests that it is essential to choose an optimum dimension that would both simplify the model and represent the elements effectively. An embedding of dimension four is found to have best of the both worlds, i.e., it reduces the complexity of the machine learning model along with capturing the intrinsic properties of the elements in the core (Figure 3(d) and S1 (a)).

The embeddings of shell elements using the model 1 shows a similar observations in Figure S2. The representation for atoms of the Cu-family (group-11) has similar embeddings and is significantly different from the Ni-family (group-10). The variability in properties going from Ni to Pd and Pt is also captured from the embeddings of the elements in shell. The vector representations of each element in the shell brilliantly enclosed this detailed information. Embeddings of the element when it is present in the core completely differs from when it is present in the shell, showing the model's ability to differentiate between core and shell elements.

After the generation of the 4-d embeddings, i.e., X_C and Y_S, the prediction of the ϵ_d for each pair of core-shell or the pseudo interaction matrix is obtained by the dot product (eq. 1) between the learned embeddings of each core and shell elements. The dimensions of X_C and Y_S are n x d and d x n, respectively, where d was found to be 4. The dot product would therefore give an n x n pseudo interaction matrix.

$$CS = X_C\, Y_S \tag{1}$$

The dot product of these representations are fed as an input to a single network to learn and predict ϵ_d (Figure 2). During the complete process, the initial two neural network frameworks learn iteratively to build representations based on which the output ϵ_d is predicted with minimal error using the single neural network. The network was trained over 200 epochs with the possibility for an early stop if the metrics did not change any longer to prevent

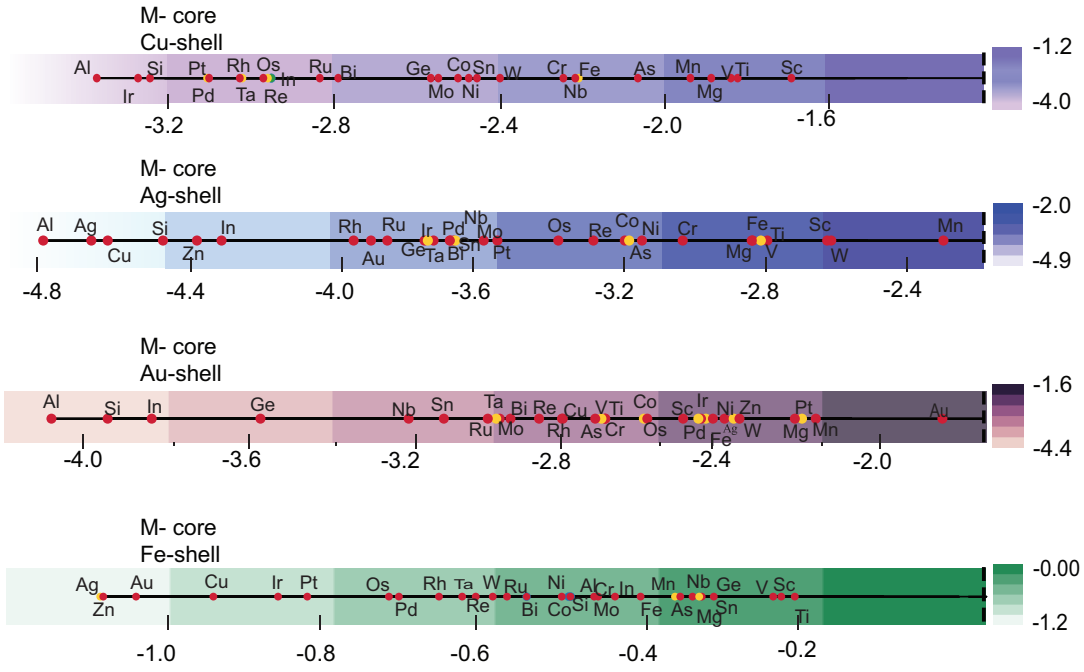

FIGURE 5 The line plots for Cu-, Ag-, Au-, and Fe- shell metals with varying core elements. The color bar indicate the range of predicted ϵ_d for each combination of core-shell.

overfitting. Training and test converge quickly, and by far not all 200 epochs have to be used as shown in Figure S1 (b and c). It is again clear from the Figure S1, model 1 performs better than the model 2.

The efficiency of a recommendation system employed is directly correlated with how accurately the metals are represented in the dataset. To comprehend the correlation between the learned representations and the predicted property, a contour plot between embeddings of different core elements with various shell elements and their corresponding ϵ_d as shown in Figure 4. The x and y axes represent the learned representations or weights. Various regions in the contour plots are divided based on their ϵ_d. The color axis represents the d-band center values. The contour plots clearly indicate that different elements cause characteristic change to the ϵ_d of shell elements. All of the shell elements included for the study exhibit these relationships; however, we have chosen to highlight Au and Ag due to their stability and wide catalytic usage. Different core elements have different embeddings for a same shell elements. As a result, their impact on the ϵ_d of the shell element also varied. For instance, the largest value of ϵ_d for Au shell is found for Al, Si, and In, and the lowest for Mg, Sc, Fe, and Mn. This analysis further suggests that the elements causing similar shift in the ϵ_d of shell atoms have similar embeddings and falls into same region of the contour plot.

Finally, the predicted ϵ_d values are plotted on a line plot against the Fermi-level, where it spans the shift in ϵ_d of a shell element with different atoms in the core. Figure 5 shows the line plot for Cu, Ag, Au, and Fe atom, in the shell with varying core elements. The ϵ_d for group-11-shell metals ranges up to -4.0 eV, whereas for Fe, it ranges only up to -1.0 eV. The model, therefore, efficiently captures this wide variability. For Au shell, the highest value for ϵ_d is for Al, Si, and In, suggesting that with the p-block elements the ϵ_d is farthest from the Fermi level, hence, weakest adsorption of reactants. However, for Cu-shell, aluminum leads to highest ϵ_d, followed by Ir. For the case of Fe-shell, Au, Ag, Zn, and Cu have the highest value of ϵ_d. On the other hand, Ag-shell has Al, Au, and Cu has highest ϵ_d. Early

transition metals and the p-bock elements such as As and Ge with these four shell elements have a ϵ_d nearest to the Fermi-level. According to the d-band model, optimum adsorption of any specie occurs when the d-band center of the catalyst is not too far or too close to the Fermi level. The range of ϵ_d for the ideal adsorption on the core-shell catalyst can be easily determined using the recommendation system model. A train/test RMSE of 0.009/0.009 was observed for the selected model. This confirms that the elemental features based representations are able to capture the properties of core and shell atoms. Further, with four dimensional embeddings we can reduce the complexity of the problem and can have a good accuracy at the same time.

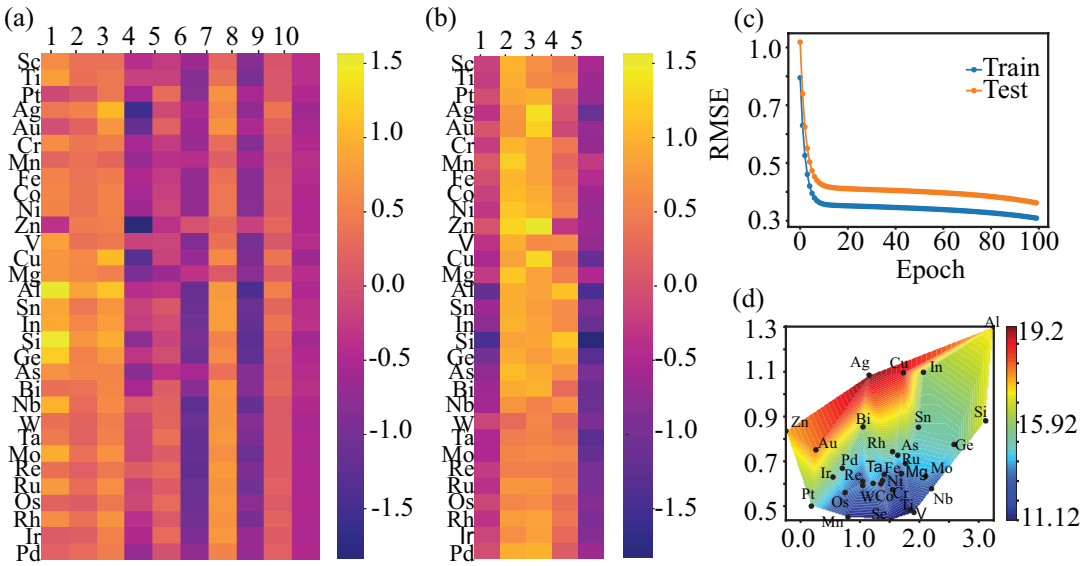

FIGURE 6 The representation heat maps at two different dimensions (a) ten-dimensional embedding representations, and (b) five-dimensional embeddings for each core element for the d-band width prediction.(c) Root mean squared error metrics of the used neural network plotted over the calculated epochs for the training set and the test set. (d) The contour plot for the d-band width prediction.

The predicted d-band center values for the core-shell nanoparticles agrees well with the d-band center calculated in various theoretical and machine learning based reports[48, 49, 50]. The ϵ_d predicted here are in the same range for various bimetals reported elsewhere[48]. For instance, the ϵ_d of copper-based bimetals is in the range of -2.0 eV to -3.5 eV, which agrees well with our predictions. However, the values of ϵ_d does not match exactly due to the structural dissimilarity between the surface and nanoparticles[48]. It is also clear that the same pair of elements have completely different ϵ_d when present in core or shell. For instance, when Pd is present in the core the ϵ_d is nearer to the Fermi level suggesting strong adsorption of reactants. On the other hand, when Pd is present in shell then the ϵ_d moves far from the Fermi level. Depending upon the type of element and its presence in the core or shell can lead to a significant variation in the ϵ_d. The results presented here capture this variability. On the basis of the prediction, combination of elements can be recomended with desired adsorption of reactants.

The recomendation system framework developed for ϵ_d is further used to predict the ϵ_w for all the core-shell systems under study. A new ϵ_w interaction matrix is generated, where each matrix element represents the ϵ_w values for a pair of core shell elements. The main task again is to predict a pseudo-interaction matrix with ϵ_w values. The

core-shell embedding for each element are learned from the same neural network framework. The 5 dimensional embedding appears to be the optimum representation of the elements with the ability to capture the intrinsic information of the elements in shell and core. The representation heat maps for various core and shell atoms were generated as shown in Figure 6(a and b). A RMSE value of 0.39/0.42 (Figure 6(c)) was observed for the train/test ϵ_w using the five dimensional embedding model. The values of ϵ_w are almost an order of magnitude higher than ϵ_d, hence the squared error (RMSE) for ϵ_w is hundred times compared to that for ϵ_d. In order to compare the values, the scaled values of ϵ_d and ϵ_w are considered. The train/test RMSE with the scaled values observed to be almost similar for both ϵ_d (0.03/0.04) and ϵ_w (0.04/0.045). Figure 6(d) shows the contour plot, where the model could predict the ϵ_w with the help of embeddings. The representations were able to separate the core elements based on their effect on the ϵ_w of the shell element, as shown in the contour plot. These results confirms the wide application of the recommendation system to predict the interdependent properties of correlated species.

While the current model provides valuable insights into the prediction of d-band centers for core-shell nanoparticles, several key areas of development can enhance its applicability and predictive power for more complex and practical systems. For instance, incorporation of structural sensitivity. The current model provides an average d-band center for core-shell nanoparticles, which, while useful as a general descriptor, may not fully capture the structural sensitivity of reaction chemistries, especially in systems with multiple unique atom types. The model can be refined by constructing interaction matrices that reflect the distinct d-band centers and adsorption behaviors of individual atom types within the nanoparticles. Further, future work will focus on extending the model to consider particle size effects, shell thickness variations, geometrical variations and trimetallic systems.

4 | SUMMARY

In conclusion, we have reported a recommendation system based approach to design core-shell nanoparticles based catalysts depending upon their electronic structure. The catalytic properties of a materials directly depends on its ability to adsorb reactant species, which in-turn depend on the ϵ_d of the catalyst. In this work, we predicted the ϵ_d of core-shell elements combinations using neural network based recommendation system. Using this model, a core-shell interaction matrix is created, where each matrix element represents ϵ_d of a unique combination of a core-shell nanoparticle. Matrix completion is employed in order to predict all the missing values of the interaction matrix using the neural network. A representation (embeddings) of each core and shell elements is generated and learned iteratively through a neural network framework with simultaneous prediction of the desired properties. The elemental features based embeddings are found to be more efficient and outperforms the randomly generated embeddings. These embeddings help differentiate between various core and shell elements and at the same time can be used to find similarities between the elements under study. An exceptionally low train/test RMSE of 0.009/0.009 was obtained. We further checked the model performance for the prediction of ϵ_w on the same data set. The model captured the uniqueness in the data and predicted the ϵ_w with a low train/test RMSE of 0.39/0.42. Using the predicted value one can easily select the range of ϵ_d and ϵ_w required to get an optimum adsorption of desired species. This approach paves the way to achieve exceptional catalytic activity tailored to specific reactions by selecting core-shell nanoparticles based on their electronic properties.

5 | DATA AVAILABILITY

The code and the data used in this work as well as the predicted d-band center for each case are available for academic use at `https://github.com/sagarwal468/Recommendationdbc`https://github.com/sagarwal468/Recommendationdbc

acknowledgements

The authors thank Materials Research Center (MRC), Supercomputer Education and Research Centre (SERC), and Solid State and Structural Chemistry Unit (SSCU), Indian Institute of Science, Bangalore for providing the required computational facilities. We thank for the support from Science and Engineering Research Board (SERB), Department of Science and Technology (DST), Government of India. The authors acknowledge DST-Nanomission programme of Department of Science and Technology, Government of India. S.A. also acknowledges Dr. Arpit Agarwal for useful discussions.

Supporting Information

Heat maps for various dimensional embeddings for core and shell metals. Contour plots for d= 6−10. Line plots for all the 31 metals used as shell to represent the d-band centre.

references

[1] Xia Y, Campbell CT, Roldan Cuenya B, Mavrikakis M, Introduction: Advanced Materials and Methods for Catalysis and Electrocatalysis by Transition Metals. ACS Publications; 2021.

[2] Wrasman CJ, Boubnov A, Riscoe AR, Hoffman AS, Bare SR, Cargnello M. Synthesis of Colloidal Pd/Au Dilute Alloy Nanocrystals and their Potential for Selective Catalytic Oxidations. JACS 2018;140(40):12930–12939.

[3] Luneau M, Shirman T, Filie A, Timoshenko J, Chen W, Trimpalis A, et al. Dilute Pd/Au Alloy Nanoparticles Embedded in Colloid-templated Porous SiO_2: Stable Au-based Oxidation Catalysts. Chem Mater 2019;31(15):5759–5768.

[4] Lee JD, Jishkariani D, Zhao Y, Najmr S, Rosen D, Kikkawa JM, et al. Tuning the Electrocatalytic Oxygen Reduction Reaction Activity of Pt−Co Nanocrystals by Cobalt Concentration with Atomic-scale Understanding. ACS Appl Mater Interfaces 2019;11(30):26789–26797.

[5] Gilroy KD, Ruditskiy A, Peng HC, Qin D, Xia Y. Bimetallic Nanocrystals: Syntheses, Properties, and Applications. Chem Rev 2016;116(18):10414–10472.

[6] Deng TS, Van Der Hoeven JE, Yalcin AO, Zandbergen HW, Van Huis MA, Van Blaaderen A. Oxidative Etching and Metal Overgrowth of Gold Nanorods within Mesoporous Silica Shells. Chem Mater 2015;27(20):7196–7203.

[7] Ahmad R, Singh AK. Synergistic core–shell interactions enable ultra-low overpotentials for enhanced CO 2 electroreduction activity. Journal of Materials Chemistry A 2018;6(42):21120–21130.

[8] van der Hoeven JE, Jelic J, Olthof LA, Totarella G, van Dijk-Moes RJ, Krafft JM, et al. Unlocking Synergy in Bimetallic Catalysts by Core-shell Design. Nat Mater 2021;20(9):1216–1220.

[9] Gawande MB, Goswami A, Asefa T, Guo H, Biradar AV, Peng DL, et al. Core-shell Nanoparticles: Synthesis and Applications in Catalysis and Electrocatalysis. Chem Soc Rev 2015;44(21):7540–7590.

[10] Bu L, Zhang N, Guo S, Zhang X, Li J, Yao J, et al. Biaxially Strained PtPb/Pt core/shell Nanoplate Boosts Oxygen Reduction Catalysis. Science 2016;354(6318):1410–1414.

[11] Wang X, Choi SI, Roling LT, Luo M, Ma C, Zhang L, et al. Palladium–platinum Core-shell Icosahedra with Substantially Enhanced Activity and Durability Towards Oxygen Reduction. Nat Comm 2015;6(1):1–8.

[12] Strasser P, Koh S, Anniyev T, Greeley J, More K, Yu C, et al. Lattice-strain Control of the Activity in Dealloyed Core–shell Fuel Cell Catalysts. Nat Chem 2010;2(6):454–460.

[13] Zhang YJ, Li SB, Duan S, Lu BA, Yang J, Panneerselvam R, et al. Probing the Electronic Structure of Heterogeneous Metal Interfaces by Transition Metal Shelled Gold Nanoparticle-enhanced Raman Spectroscopy. J Phys Chem C 2016;120(37):20684–20691.

[14] Ahmadi M, Behafarid F, Cui C, Strasser P, Cuenya BR. Long-range Segregation Phenomena in Shape-selected Bimetallic Nanoparticles: Chemical State Effects. ACS Nano 2013;7(10):9195–9204.

[15] Zugic B, Wang L, Heine C, Zakharov DN, Lechner BA, Stach EA, et al. Dynamic Restructuring Drives Catalytic Activity on Nanoporous Gold–Silver Alloy Catalysts. Nat Mater 2017;16(5):558–564.

[16] Montemore MM, Medlin JW. Scaling Relations Between Adsorption Energies for Computational Screening and Design of Catalysts. Catal Sci Tech 2014;4(11):3748–3761.

[17] Wang S, Temel B, Shen J, Jones G, Grabow LC, Studt F, et al. Universal Bronsted-evans-polanyi relations for C–C, C–O, C–N, N–O, N–N, and O–O Dissociation Reactions. Catal Lett 2011;141(3):370–373.

[18] Greeley J. Theoretical Heterogeneous Catalysis: Scaling Relationships and Computational Catalyst Design. Ann Rev Chem Biomol Eng 2016;7:605–635.

[19] Zhao ZJ, Liu S, Zha S, Cheng D, Studt F, Henkelman G, et al. Theory-guided Design of Catalytic Materials Using Scaling Relationships and Reactivity Descriptors. Nat Rev Mater 2019;4(12):792–804.

[20] Nørskov JK, Abild-Pedersen F, Studt F, Bligaard T. Density Functional Theory in Surface Chemistry and Catalysis. Proc Natl Acad Sci 2011;108(3):937–943.

[21] Hammer B, Norskov JK. Why Gold is the Noblest of all the Metals. Nature 1995;376(6537):238–240.

[22] Kitchin JR, Nørskov JK, Barteau MA, Chen J. Role of Strain and Ligand Effects in the Modification of the Electronic and Chemical Properties of Bimetallic Surfaces. Phys Rev Lett 2004;93(15):156801.

[23] Vojvodic A, Nørskov J, Abild-Pedersen F. Electronic Structure Effects in Transition Metal Surface Chemistry. Top Catal 2014;57(1):25–32.

[24] Xin H, Vojvodic A, Voss J, Nørskov JK, Abild-Pedersen F. Effects of d-band Shape on the Surface Reactivity of Transition-metal Alloys. Phys Rev B 2014;89(11):115114.

[25] Ma X, Xin H. Orbitalwise Coordination Number for Predicting Adsorption Properties of Metal Nanocatalysts. Phys Revi Lett 2017;118(3):036101.

[26] Calle-Vallejo F, Loffreda D, Koper M, Sautet P. Introducing Structural Sensitivity into Adsorption–energy Scaling Relations by Means of Coordination Numbers. Nat Chem 2015;7(5):403–410.

[27] Visikovskiy A, Matsumoto H, Mitsuhara K, Nakada T, Akita T, Kido Y. Electronic d-band Properties of Gold Nanoclusters Grown on Amorphous Carbon. Phys Rev B 2011;83(16):165428.

[28] Agarwal S, Singh AK. Electroreduction of CO2 with Tunable Selectivity on Au–Pd Bimetallic Catalyst: A First Principle Study. ACS Applied Materials & Interfaces 2022;14(9):11313–11321.

[29] Agarwal S, Kumar R, Arya R, Singh AK. Rational design of single-atom catalysts for enhanced electrocatalytic nitrogen reduction reaction. The Journal of Physical Chemistry C 2021;125(23):12585–12593.

[30] Ramprasad R, Batra R, Pilania G, Mannodi-Kanakkithodi A, Kim C. Machine Learning in Materials Informatics: Recent Applications and Prospects. npj Comp Mater 2017;3(1):1–13.

[31] Back S, Yoon J, Tian N, Zhong W, Tran K, Ulissi ZW. Convolutional Neural Network of Atomic Surface Structures to Predict Binding Energies for High-throughput Screening of Catalysts. J Phys Chem Lett 2019;10(15):4401–4408.

[32] Tran K, Ulissi ZW. Active Learning Across Intermetallics to Guide Discovery of Electrocatalysts for CO_2 Reduction and H_2 Evolution. Nat Catal 2018;1(9):696–703.

[33] Kumar R, Singh AK. Chemical hardness-driven interpretable machine learning approach for rapid search of photocatalysts. npj Computational Materials 2021;7(1):197.

[34] Juneja R, Singh AK. Unraveling the role of bonding chemistry in connecting electronic and thermal transport by machine learning. Journal of materials chemistry A 2020;8(17):8716–8721.

[35] Mukherjee M, Satsangi S, Singh AK. A statistical approach for the rapid prediction of electron relaxation time using elemental representatives. Chemistry of Materials 2020;32(15):6507–6514.

[36] Barik RK, Singh AK. Accelerated Discovery of the Valley-Polarized Quantum Anomalous Hall Effect in MXenes. Chemistry of Materials 2021;33(16):6311–6317.

[37] Melville P, Sindhwani V. Recommender Systems. Encycl Mach Learn 2010;1:829–838.

[38] Burke R, Felfernig A, Göker MH. Recommender Systems: An Overview. Ai Maga 2011;32(3):13–18.

[39] Hayashi H, Hayashi K, Kouzai K, Seko A, Tanaka I. Recommender System of Successful Processing Conditions for New Compounds Based on a Parallel Experimental Data Set. Chem Mater 2019;31(24):9984–9992.

[40] Suzuki K, Ohura K, Seko A, Iwamizu Y, Zhao G, Hirayama M, et al. Fast Material Search of Lithium Ion Conducting Oxides Using a Recommender System. J Mater Chem A 2020;8(23):11582–11588.

[41] Park NH, Zubarev DY, Hedrick JL, Kiyek V, Corbet C, Lottier S. A Recommender System for Inverse Design of Polycarbonates and Polyesters. Macromolecules 2020;53(24):10847–10854.

[42] Seko A, Hayashi H, Kashima H, Tanaka I. Matrix-and Tensor-based Recommender Systems for the Discovery of Currently Unknown Inorganic Compounds. Phys Rev Mater 2018;2(1):013805.

[43] Seko A, Hayashi H, Tanaka I. Compositional Descriptor-based Recommender System for the Materials Discovery. J Chem Phys 2018;148(24):241719.

[44] Zhou Q, Tang P, Liu S, Pan J, Yan Q, Zhang SC. Learning Atoms for Materials Discovery. Proc Natl Acad Sci 2018;115(28):E6411–E6417.

[45] Kresse G, Furthmüller J. Efficiency of Ab-initio Total Energy Calculations for Metals and Semiconductors using a Plane-wave Basis set. Comput Mater Sci 1996;6(1):15–50.

[46] Kresse G, Joubert D. From Ultrasoft Pseudopotentials to the Projector Augmented-wave Method. Phys Rev B 1999;59(3):1758.

[47] Perdew JP, Burke K, Ernzerhof M. Generalized Gradient Approximation Made Simple. Phys Rev Lett 1996;77(18):3865.

[48] Takigawa I, Shimizu Ki, Tsuda K, Takakusagi S. Machine-learning Prediction of the d-band center for Metals and Bimetals. RSC Adv 2016;6(58):52587–52595.

[49] Hammer B, Nørskov JK. Theoretical Surface Science and Catalysis–Calculations and Concepts. In: Adv. Catal., vol. 45 Elsevier; 2000.p. 71–129.

[50] Ruban A, Hammer B, Stoltze P, Skriver HL, Nørskov JK. Surface Electronic Structure and Reactivity of Transition and Noble Metals. J Mol Catal A Chem 1997;115(3):421–429.